Biofabrication

International Edition: DOI: 10.1002/anie.201700153
German Edition: DOI: 10.1002/ange.201700153

Control of Nanoparticle Release Kinetics from 3D Printed Hydrogel Scaffolds

Bernhard Baumann[+], Tomasz Jungst[+], Simone Stichler, Susanne Feineis, Oliver Wiltschka, Matthias Kuhlmann, Mika Lindén, and Jürgen Groll**

Abstract: *The convergence of biofabrication with nanotechnology is largely unexplored but enables geometrical control of cell-biomaterial arrangement combined with controlled drug delivery and release. As a step towards integration of these two fields of research, this study demonstrates that modulation of electrostatic nanoparticle–polymer and nanoparticle–nanoparticle interactions can be used for tuning nanoparticle release kinetics from 3D printed hydrogel scaffolds. This generic strategy can be used for spatiotemporal control of the release kinetics of nanoparticulate drug vectors in biofabricated constructs.*

Additive manufacturing (AM), often referred to as 3D printing, exhibits great potential for tissue engineering and regenerative medicine, especially in biofabrication where cells and materials are processed simultaneously into composite structures with hierarchical organization.[1] A key challenge is the development of materials that are printable, which maintain high shape fidelity, and enhance (stem-) cell viability, proliferation, and differentiation post-processing.[2a,b] Hydrogels are predominantly used in this context,[3a–c] and recently a number of promising strategies have been proposed, such as thiol-ene dimerization as a stabilizing cross-linking method,[4] double cross-linking using reversible covalent bond formation,[5] core–shell printing for reduced viscosity,[6] purely physical hydrogels,[7] and printing into self-healing support gels.[8]

[*] B. Baumann,[+] O. Wiltschka, Prof. Dr. M. Lindén
Institute of Inorganic Chemistry II
University of Ulm
Albert-Einstein-Allee 11, 89081 Ulm (Germany)
E-mail: mika.linden@uni-ulm.de

T. Jungst,[+] S. Stichler, S. Feineis, Dr. M. Kuhlmann, Prof. Dr. J. Groll
Department of Functional Materials in Medicine and Dentistry and Bavarian Polymer Institute (BPI)
University of Würzburg
Pleicherwall 2, 97070 Würzburg (Germany)
E-mail: juergen.groll@fmz.uni-wuerzburg.de

[+] These authors contributed equally to this work.

Supporting information and the ORCID identification number(s) for the author(s) of this article can be found under: http://dx.doi.org/10.1002/anie.201700153.

Furthermore, cell behavior can be influenced by chemical cues especially addressing cell phenotype stability, stem cell proliferation, and differentiation. Nanotechnology offers an intriguing possibility to endow 3D printed structures with tailored and eventually sequential drug-release capacities over desired time frames. This combination of biofabrication with controlled drug-delivery systems is yet largely unexplored.[9] A series of recent papers shows the possibility for cell-directed drug release from mesoporous silica nanoparticles (MSNs) serving as the drug carriers either from 2D MSN films[10] or from MSNs that have been adsorbed onto the surface of electrospun 3D scaffolds.[11] Small molecular hydrophobic drugs are retained in the particles with no premature release,[12] but the drugs are released intracellularly after the MSNs have been taken up by the cells. It has also been shown that MSNs can be embedded into hydrogels to mediate diffusion-controlled drug release.[13a,b]

Herein we demonstrate that the release of MSNs from 3D printed hydrogel scaffolds can easily be modulated over times from days to weeks through tuning of electrostatic nanoparticle–polymer and nanoparticle–nanoparticle interactions. Thus, our results reveal a strategy towards controlled sequential drug release from 3D printed hydrogel constructs.

Spherical MSNs with an approximate size of 350 nm, exhibiting a narrow size distribution and high surface areas (Figure S1 in the Supporting Information), were synthesized according to literature procedures.[15] The surface of MSNs was functionalized with either amino (MSN-NH_2) or carboxy groups (MSN-COOH) leading to positively and negatively charged particles under the studied conditions (Table S1). For examination of particle mobility and release, MSN-NH_2 particles were labeled with the red fluorescent ATTO 647N dye, and MSN-COOH were labelled with the green fluorescent ATTO 488 dye. Thiol-ene cross-linked polyglycidols and hyaluronic acid (HA, 1.36 MDa) was used as the hydrogel matrix.[4]

As rheology is a crucial evaluation criterion for the development of inks for 3D hydrogel printing, we first assessed whether addition of the MSNs to the different formulations affects the rheological properties. All measurements were performed using formulations without a photoinitiator to prevent cross-linking of the network during the measurement. Rotational measurements revealed shear thinning behavior for all materials with only small shifts for MSN containing inks (Figure 1a) indicating that the addition of MSNs had no significant influence on the shear thinning properties. To simulate the recovery of the material after being dispensed, an experiment with an alteration of high (5 s^{-1}) and low shear rates (0.01 s^{-1}) was carried out (Fig-

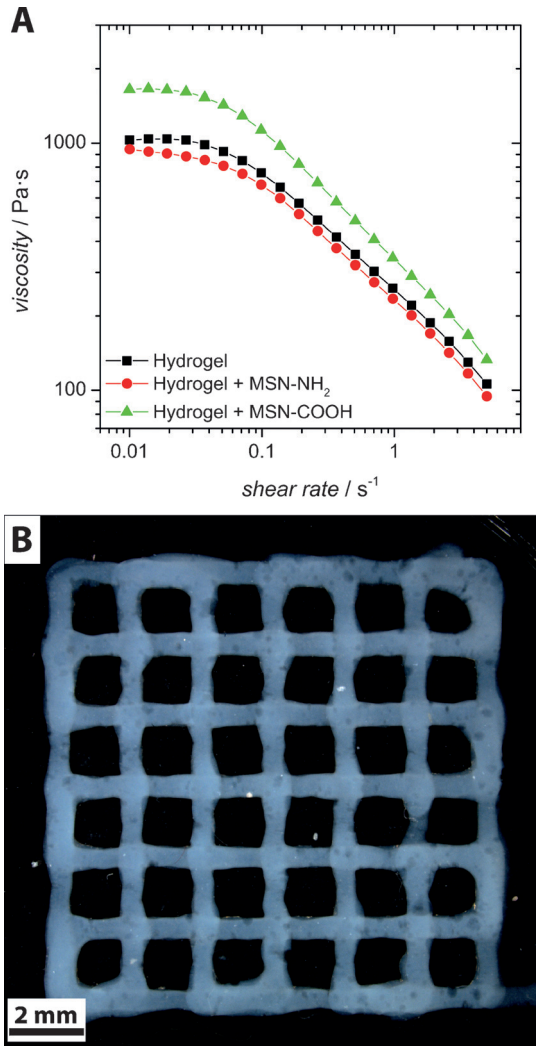

Figure 1. a) Viscosity over shear rate for different systems measured with a rheometer in cone-plate geometry under rotation. b) Stereomicroscopic image showing a top view of a four-layer construct. The diameter of the strands was 627 ± 31 µm.

ure S7) demonstrating a rapid recovery of the formulation. Also in this case the influence of the MSNs was minor. Further, frequency sweeps were performed to analyze the viscoelastic ink properties showing that the particles did not significantly influence the ink 's viscoelastic behavior (see Figure S6).

In accordance with the rheological evaluations the MSNs did not change the printability of the inks and all formulations could be printed under identical conditions (Supporting Information). Constructs with a size of $12 \times 12\ mm^2$ and a height of about 3 mm were obtained by printing 16 layers one on top of the other (Figure S9). Mixing of the MSN containing formulation led to the formation of small air bubbles (Figure 1 B), which however did not negatively influence the printability.

In all cases, an even distribution of particles could be observed over the whole examined cross-section of the hydrogel (Figure 2 A–C). A representative confocal laser microscopy (CLM) image of a printed strand containing a mixture of MSN-NH_2 and MSN-COOH particles present in equal amounts is presented in Figure 2 D). Macroscopically, a homogeneous distribution of both particles was observed, and the co-localization of green and red fluorescence indicates the formation of small particle agglomerates by attractive electrostatic particle interactions.

To investigate the role of electrostatic interactions on the MSN mobility in the negatively charged polymer network, hydrogel strands that contained either MSN-NH_2 or MSN-COOH particles were printed either in perpendicular orientation on top of each other or in parallel orientation next to each other with a defined distance without direct contact (Figure 3, Figure S8). The scaffolds were then immersed in PBS buffer and the particle migration was monitored over time. After only one day, migration of positively charged MSN-NH_2 into the complete volume of the strand containing negatively charged MSN-COOH was observed. This effect was sustained and was more pronounced after storage in PBS for six weeks. A homogenous distribution of MSN-NH_2 within both strands indicates that the particle motion for positively charged particles into the strand loaded with negatively charged particles is rapid when the strands are in direct contact. In contrast, the migration of MSN-COOH was negligible even after six weeks. Since the overall net-charge of both strands is negative because of the high charge density of HA, these effects are both driven by electrostatic forces. While the positively charged particles are attracted by the higher negative charge density in the other strand, the driving force for the negatively charged particles to migrate into the other strand is not sufficient.

In the non-contact case (Figure 3, bottom), the MSNs cannot directly migrate into the other strand but must first be released into the surrounding liquid before being taken up by the other strand. In this case, no exchange of particles could be observed for both strands after one day of incubation. After six weeks of incubation MSN-NH_2 particles could be detected in the opposite strand, with higher fluorescence intensity at the side where the two strands face each other. MSN-COOH particles were detectable to a lesser extent in the other strand. Also these findings can be explained by electrostatics. MSN-NH_2 particles are released slowly from the strands, presumably together with HA that is not covalently immobilized in the hydrogel. Once they are released, they are attracted to the strand exhibiting a higher net-negative charge. Repulsion between the negatively charged MSN-COOH and the hydrogel favors release of these particles into the surrounding buffer solution. Owing to the overall negative net charge of both strands, a re-uptake of those particles into either strand is less probable than suspension of the particles or sedimentation.

MSN mobility can thus be influenced both by particle charge and by the geometry of the printed construct. This may be exploited for tailored uptake of MSNs by cells. To qualitatively investigate this, C2C12 cells were seeded beside different MSN-containing cast hydrogels without direct contact between the analyzed cells and the scaffold at any time (Figure 4). MSN-COOH were readily taken up by cells at all three times tested. In contrast, for MSN-NH_2 only at day 5 a stronger uptake of MSN-NH_2 could be observed. As

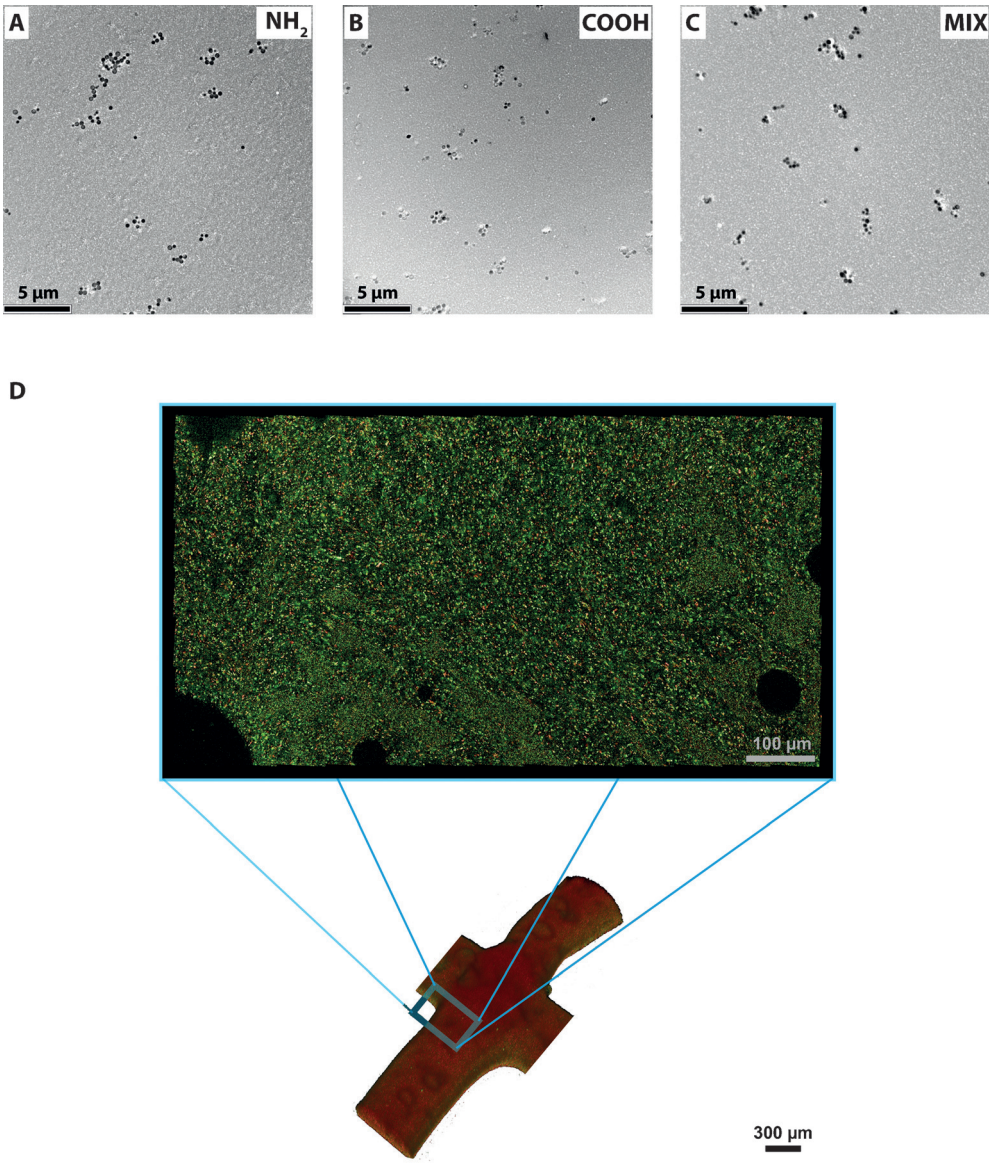

Figure 2. Particle distribution within printed constructs a)–c) Transmission electron microscopy images showing particle distribution within the printed hydrogel network. a) MSN-COOH, b) MSN-NH_2, c) MSN-COOH and MSN-NH_2, d) Confocal laser microscopy image of a section through a printed construct containing a mixture of positively (MSN-NH_2, ATTO 647 N labeled, red) and negatively (MSN-COOH, ATTO 488 labeled, green) charged particles.

already shown in literature positively charged MSN are taken up by cells much more rapidly and efficiently than negatively charged particles.[14a,b] We could also confirm this behavior for C2C12 cells with the charged MSN used in this study in a classical 2D cell culture (Figure S10).

To exclude any influence of surface-chemistry-related differences in agglomeration on cellular uptake, the stability of the respective particle dispersions in FCS-containing cell culture media was studied. As shown in Figure S11, no MSN agglomeration is expected for any of the MSNs, and thus influences of differences in aggregation state between the two types of MSNs on cellular uptake kinetics can be excluded.

Hence, in accordance with the discussion above, the negatively charged MSN-COOH particles are rapidly released from the scaffold into the medium and can thus be taken up by the C2C12 cells anywhere in the well plate, whereas the release of positively charged MSN-NH_2 was significantly delayed. Accordingly, the delayed uptake into the cells directly corresponds to a delayed release of these particles from the hydrogel into the medium. For hydrogels including a mixture of MSN-COOH and MSN-NH_2 (MSN-Mix) no significant uptake in C2C12 cells between 1 and 5 days could be observed. This corresponds to the observation of particle aggregation within the hydrogel owing to electrostatic attraction (Figure 2) which leads to hindered ability of these aggregates to migrate into the medium.

To confirm that the observed differences in particle release kinetics indeed are related to the differences in particle surface chemistry, small gold nanoparticles with corresponding surface functionalities, AuNP-COOH and AuNP-NH_2 (preparation and characterization see Supporting Information) where mixed with the aforementioned printable hydrogel system instead of MSN. An assessment of the release kinetics of the gold particles was qualitatively performed by UV/Vis spectroscopy (Figure S4) and quantified by inductively coupled plasma mass spectroscopy (ICP-MS, Figure 5) after 1, 5, and 9 days of incubation. These measurements show that negatively charged particles were released in higher amounts than the positively charges ones for all times. While the amount of particles released decreased with time for negatively charged particles, the positively charged particles were released without significant rate change over time. This could be explained by the lower amount of particles left in the gel as the supernatant was changed at each time point and thus by a lower diffusion gradient between gel and supernatant.

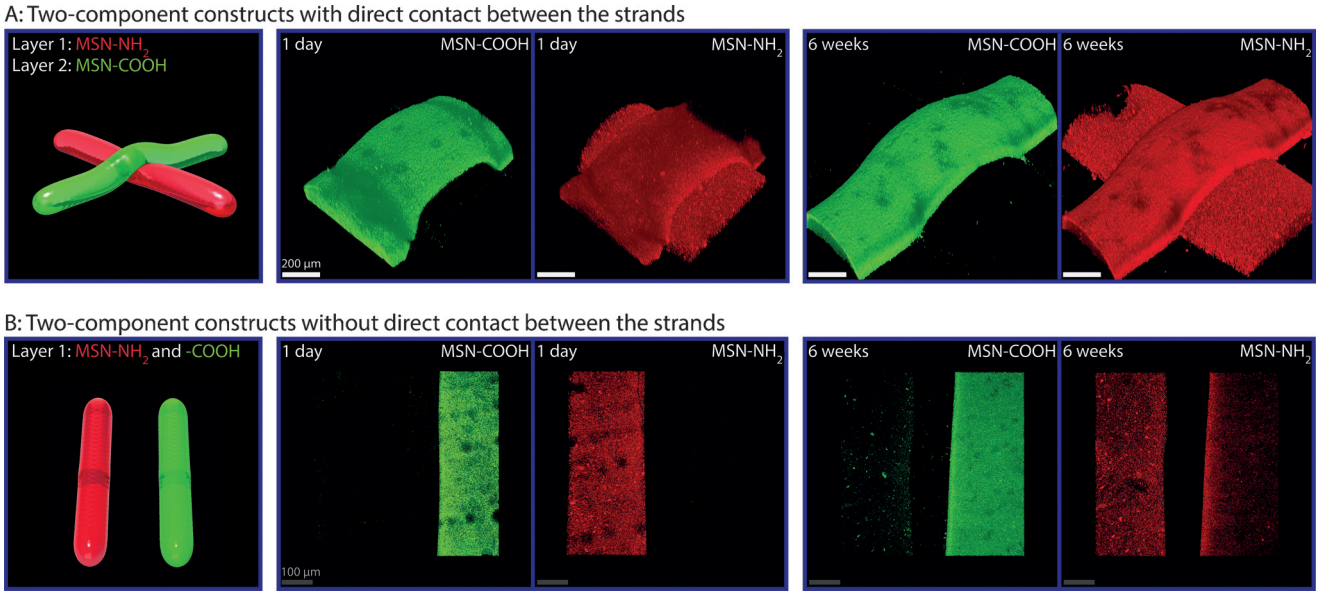

Figure 3. Particle migration into hydrogels with and without direct contact. a) 3D reconstruction of a construct made from two components, MSN-NH_2 and MSN-COOH containing ink, with a direct contact setup of orthogonal filaments. The image on the very left side shows a model of the construct as it would appear just after printing. The other images show confocal 3D reconstructions of real constructs at different times (1 day and 6 weeks) after printing. In these images the signals of the MSN-COOH and the MSN-NH_2 are displayed separately. b) The same set of figures for a construct where two parallel strands were printed that did not have direct contact.

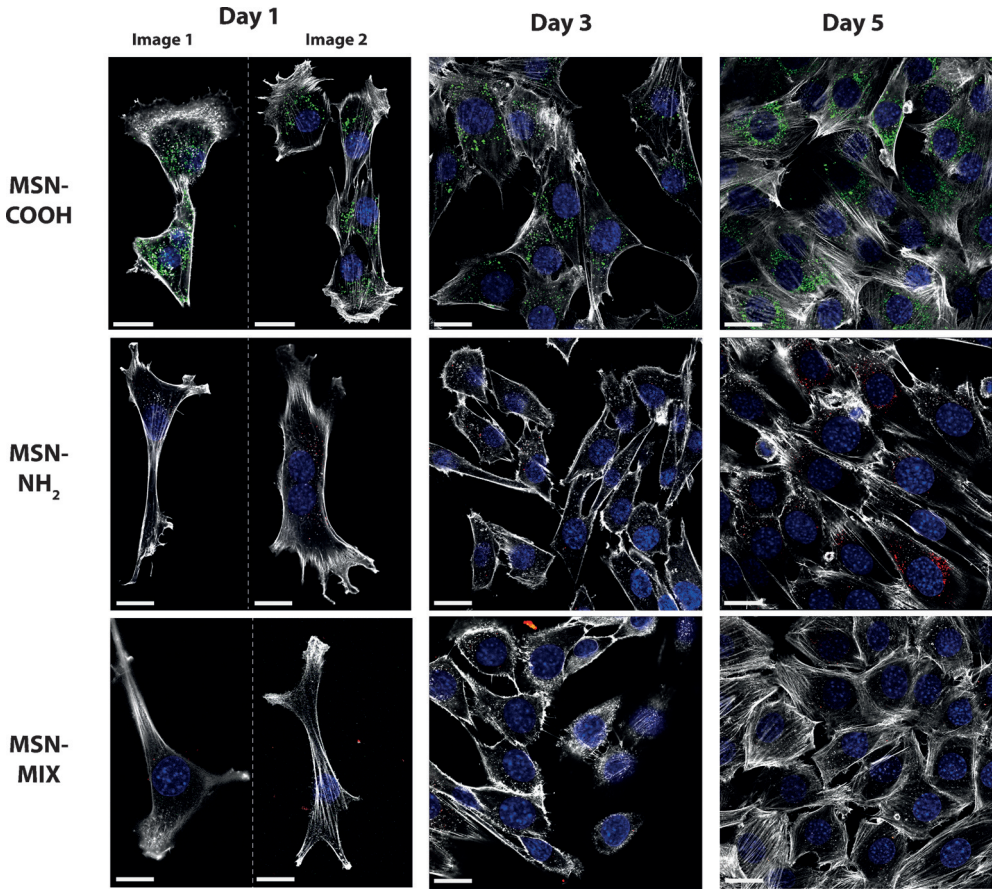

Figure 4. Uptake of different functionalized MSN by C2C12 cells (1, 3, and 5 days) after release from crafted scaffolds. Cells were stained using Phalloidin-TRITC for the cytoskeleton (white) and DAPI for the nucleus (blue). Depending on the surface functionalization particles are shown in red (MSN-NH_2) or green (MSN-COOH). Confocal laser microscopy was performed using a confocal laser microscope with identical microscope settings and laser intensity. All scale bars correspond to 20 µm.

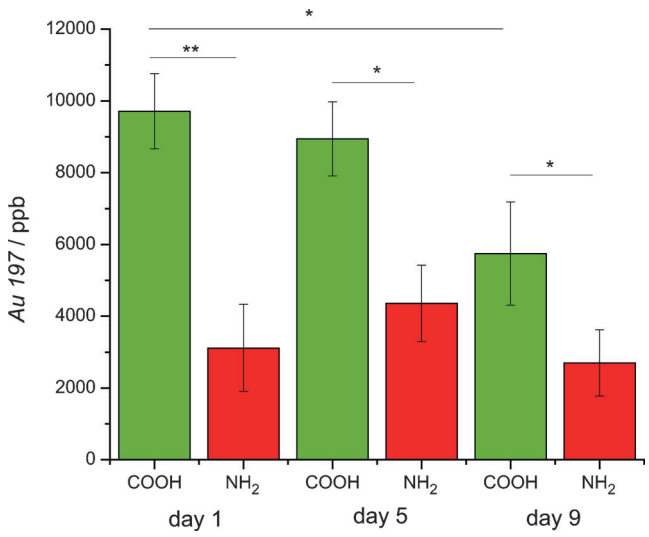

Figure 5. Inductively coupled plasma mass spectroscopy (ICP-MS) of gold nanoparticles functionalized with carboxy- and amino-groups. For each measurement the supernatant was used for ICP-MS analysis and was therefore completely exchanged each time.

We show that charged MSN do not significantly affect the rheological properties of a printable hydrogel based on neutral polyglycidol precursors and negatively charged hyaluronic acid. After printing, electrostatic interactions between the nanoparticles and the hyaluronic acid determine the release kinetics of the nanoparticles from the printed structure. This effect was quantified using surface charged gold nanoparticles, underlining that rational control of electrostatic nanoparticle–polymer and nanoparticle–nanoparticle interactions independent of nanoparticle composition allows tuning of nanoparticle mobility in and release from printed hybrid nanoparticle–polymer hydrogel scaffolds. These results are of interest for controlling the release kinetics of drug vectors from printed scaffolds, and could be used for design of scaffolds exhibiting sequential release properties for biofabrication.

Experimental Section

MSN synthesis, functionalization and characterization[15] as well as synthesis of the allyl- and thiol-functional polyglycidols[4] were performed according to literature (see Supporting Information for details).

For preparation of the ink, half of the MSN-PBS sol (10 mg mL^{-1}) was mixed with allyl-functional polyglycidol (PG) followed by addition of 0.05 wt % photoinitiator (Irgacure 2959). Thiol-functional PG was dissolved in the other half of the MSN-PBS sol and both sols were combined to yield an equimolar functional group ratio of 1:1 (allyl:SH). Subsequently 3.5 wt % hyaluronic acid (1.36 MDa) was added and a final PG concentration of 17 wt % was reached.

Details of the rheological examination can be found in the Supporting Information. Printing was performed with a 3D bioprinter (3DDiscovery, regenHU) using an electromagnetic valve dispenser (cell friendly printhead CF-300N/H) equipped with a 300 μm inner diameter valve and nozzle at 800 μs valve opening time, a dosing distance of 45 μm and a print speed of 15 mm min^{-1} at 3.4 bar. For double printing (Figure S8), the second ink type was processed with a syringe dispenser (pneumatic driven printhead DD-135N) equipped with a 330 μm inner diameter flat tipped precision needle (Nordson EFD, 6.35 mm length) at 1.5 bar and 15 mm min^{-1}. The constructs were UV-crosslinked during printing (bluepoint 4, hönle; for details see Supporting Information). Cell culture studies are described in the Supporting Information.

Acknowledgements

This work was financially supported by the European Community's 7th Framework Programme under grant agreement 309962 (HydroZONES) and the European Research Council under grant agreement 617989 (Design2Heal). The biological division at ILM Ulm and the department for tissue engineering and regenerative medicine at the University of Würzburg are thanked for providing access to the confocal laser microscopes and for excellent technical assistance. We thank Daimon Hall (CGI, carbonandneon.com) for support with the illustrations.

Conflict of interest

The authors declare no conflict of interest.

Keywords: biofabrication · charge interaction · controlled release · gold nanoparticles · mesoporous silica nanoparticles

How to cite: *Angew. Chem. Int. Ed.* **2017**, *56*, 4623–4628
Angew. Chem. **2017**, *129*, 4694–4699

[1] J. Groll, T. Boland, T. Blunk, J. A. Burdick, D.-W. Cho, P. D. Dalton, B. Derby, G. Forgacs, Q. Li, V. A. Mironov, L. Moroni, M. Nakamura, W. Shu, S. Takeuchi, G. Vozzi, T. B. F. Woodfield, T. Xu, J. J. Yoo, J. Malda, *Biofabrication* **2016**, *8*, 013001.
[2] a) B. Derby, *Science* **2012**, *338*, 921; b) S. V. Murphy, A. Atala, *Nat. Biotechnol.* **2014**, *32*, 773.
[3] a) T. Billiet, M. Vandenhaute, J. Schelfhout, S. Van Vlierberghe, P. Dubruel, *Biomaterials* **2012**, *33*, 6020; b) J. Malda, J. Visser, F. P. Melchels, T. Jüngst, W. E. Hennink, W. J. A. Dhert, J. Groll, D. W. Hutmacher, *Adv. Mater.* **2013**, *25*, 581; c) T. Jungst, W. Smolan, K. Schacht, T. Scheibel, J. Groll, *Chem. Rev.* **2016**, *116*, 1496.
[4] S. Stichler, T. Jungst, M. Schamel, I. Zilkowski, M. Kuhlmann, T. Böck, T. Blunk, J. Teßmar, J. Groll, *Ann. Biomed. Eng.* **2017**, *45*, 273.
[5] T. Zehnder, B. Sarker, A. R. Boccaccini, R. Detsch, *Biofabrication* **2015**, *7*, 025001.
[6] C. Colosi, S. R. Shin, V. Manoharan, S. Massa, M. Costantini, A. Barbetta, M. R. Dokmeci, M. Dentini, A. Khademhosseini, *Adv. Mater.* **2016**, *28*, 677.
[7] K. Schacht, T. Jungst, M. Schweinlin, A. Ewald, J. Groll, T. Scheibel, *Angew. Chem. Int. Ed.* **2015**, *54*, 2816; *Angew. Chem.* **2015**, *127*, 2858.
[8] C. B. Highley, C. B. Rodell, J. A. Burdick, *Adv. Mater.* **2015**, *27*, 5075.
[9] J. Rosenholm, J. Zhang, M. Lindén, C. Sahlgren, *Nanomedicine* **2016**, *11*, 391.
[10] D. Böcking, O. Wiltschka, J. Niinimäki, H. Shokry, R. Brenner, M. Lindén, C. Sahlgren, *Nanoscale* **2014**, *6*, 1490.
[11] H. Shokry, U. Vanamo, O. Wiltschka, J. Niinimäki, M. Lerche, K. Levon, M. Lindén, C. Sahlgren, *Nanoscale* **2015**, *7*, 14434.

[12] E. von Haartman, D. Lindberg, N. Prabhakar, J. Rosenholm, *Eur. J. Pharm. Sci.* **2016**, *95*, 17.
[13] a) N. Kehr, E. Prasetyanto, K. Benson, B. Ergün, A. Galstyan, H. J. Galla, *Angew. Chem. Int. Ed.* **2013**, *52*, 1156 – 1160; *Angew. Chem.* **2013**, *125*, 1194 – 1198; b) C. P. Silveira, L. M. Apolinário, W. J. Fávaro, A. J. Paula, N. Durán, *ACS Biomater. Sci. Eng.* **2016**, *2*, 1190.
[14] a) T. Chung, S. Wu, M. Yao, C. Lu, Y. Lin, Y. Hung, C. Mou, Y. Chen, D. Huang, *Biomaterials* **2007**, *28*, 2959 – 2966; b) I. Slowing, B. Trewyn, V. Lin, *J. Am. Chem. Soc.* **2006**, *128*, 14792.
[15] J. Rosenholm, A. Meinander, E. Peuhu, R. Niemi, J. E. Eriksson, C. Sahlgren, M. Lindén, *ACS Nano* **2009**, *3*, 197.

Manuscript received: January 6, 2017
Final Article published: March 22, 2017

